Pulse Processing for the PET Liquid Xenon Multiwire Ionisation Chamber

P. Crespo[1*], J. van der Marel[1], V. Chepel[1], M.I. Lopes[1], Dinis Santos[2], L. Janeiro[1], V. Solovov[1], R. Ferreira Marques[1] and A.J.P.L. Policarpo[1]

[1]LIP-Coimbra and Physics Department of the University of Coimbra, 3000 Coimbra, Portugal
[2]Electronics and Telecommunications Department of the University of Aveiro, 3810 Aveiro, Portugal

Abstract

The readout and data acquisition systems designed for a first prototype of liquid xenon position sensitive gamma ray detector for Positron Emission Tomography is described. The problem of measurement of the gamma ray energy in the gridless multiwire ionisation chamber is considered. A previously suggested drift time based correction algorithm, allowing correction of the amplitude spectra for the contribution of positive ions, is experimentally tested. First ionisation spectra, with an energy resolution of 15-17%, are presented. A pulse shape discrimination method for rejecting the induction cross-talk between the wires, improving energy resolution and allowing the unambiguous identification of Compton scattered events in the detector, is described.

I. Introduction

A position-sensitive liquid xenon detector is being developed for Positron Emission Tomography [1-3]. Liquid xenon fits very well the requirements of PET. It is an excellent scintillator, having a light yield similar to NaI(Tl), with decay times of ~3 ns and ~30ns. Furthermore, the electrons released by the γ-ray can be easily extracted and collected, allowing the use of various methods of position determination.

By combining the scintillation and ionisation signals of liquid xenon, two-dimensional positioning with a precision of a few millimetres and time resolution in the nanosecond range were achieved [2,4]. This allows the transaxial and radial coordinates to be measured and, therefore, the parallax problem to be solved.

However, determination of the energy deposited by a γ-ray in the multiwire ionisation chamber meets with some difficulties. The demand of high count rate in a PET detector imposes the segmentation of the chamber in order to reduce the electron collection time. On the other hand, the requirement for minimum dead space does not allow the use of a Frisch grid to eliminate the contribution of slowly moving positive ions to the measured ionisation signals. As found in our previous study [5], this results in a strong dependence of the amplitude and shape of the charge signals on the position of primary ionisation, resulting in degradation of the energy resolution. Simulation also shows that there is a correlation between the electron drift time and the signal amplitude [5]. Therefore, the implementation of a time based amplitude correction algorithm can significantly improve resolution.

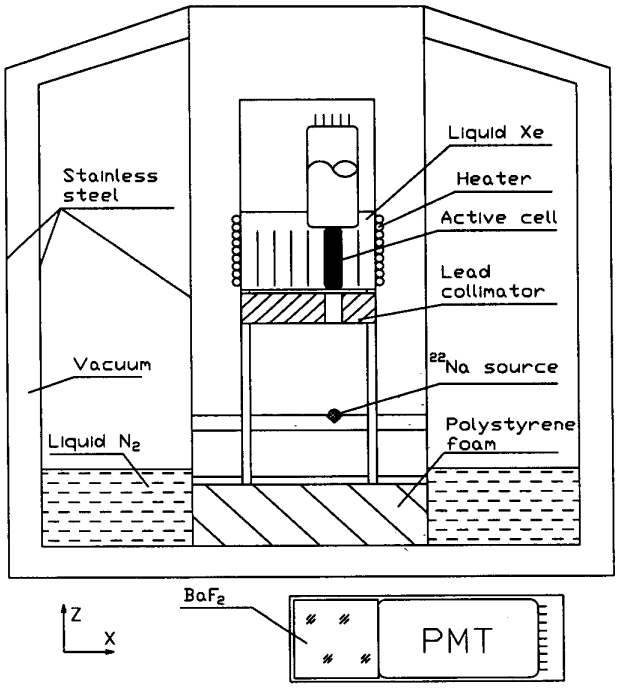

Figure 1: Schematic of the experimental set-up .

In this work, we describe the electronic and data acquisition system designed to read out the liquid xenon multiwire ionisation chamber and allow the above correction to be performed. The experimental results on energy resolution for 511 keV γ-rays obtained with this system are also reported.

* Corresponding author, Vitaly@lipc.fis.uc.pt

0-7803-5021-9/99/$10.00 © 1999 IEEE.

II. Liquid Xenon Chamber and Experimental Set-up

The set-up used for the measurements is schematically drawn in Fig.1. The liquid xenon multiwire detector, built for test purposes and previously described in detail in [2,3], consists of a stainless steel box with six multiwire cells. These cells, 1 cm wide (along the x-direction) are separated by stainless steel cathode planes 0.5 mm thick. The height of each cell (z-direction) is 5 cm and its length (y-direction) 6 cm. The anode plane in the middle of each cell is formed by twenty stainless steel wires (ϕ=50 μm) stretched along the y-direction with a pitch of 2.5 mm (z). These anode wires are connected in pairs to low-noise charge sensitive preamplifiers [6] that are mounted directly outside the chamber on the ceramic feedthroughs for reducing the noise, thus being operated at low temperature. The anode wires are at ground potential and the cathode planes are at a negative voltage, usually -1000 V.

Two Hamamatsu R1668 photomultipliers are mounted inside the chamber just above the cell. They have 30 mm diameter quartz windows and bialkali photocathodes. Positive high voltage is applied to the anodes, so that the photocathodes can be at ground potential. Two signals were read from each PMT tube, one taken from the last dynode for fast timing and the other from the anode for amplitude analysis. The windows of the PMTs are immersed in liquid xenon for a good optical contact.

For the tests, only one multiwire cell was completely set up with PMTs and read-out electronics. To assure that mainly this cell was irradiated, a 3 cm thick lead collimator with a hole of 8×8 mm^2 was placed 2.3 cm beneath the chamber and 8.3 cm above a ^{22}Na source. The hole aligned with the centre of the active cell. To avoid that light coming from other cells is detected by the PMTs, the latter were shielded from those cells.

The LXe detector, the collimator and the ^{22}Na-source are mounted on a rigid frame to assure a proper alignment. This frame, in turn, is placed into the cryostat containing liquid nitrogen. An electrical heater wound around the chamber and gas jacket between the detector and the cryostat allow operation of the detector at a temperature of around -100 °C. The gaseous xenon was purified by passing it through an Oxisorb column. The electron lifetime was measured to be >20 μs (limit corresponding to the upper sensitivity of the impurity monitor used in this measurement), which is sufficient for operating the chamber. We refer to [7] for details about our purification and cryogenic systems, as well as for discussion of the purity problem.

The ^{22}Na source emits positrons and 1.27 MeV γ-rays. Pairs of 511 keV γ-rays due to positrons annihilating in the source substrate (an aluminium plate) were selected by putting the two

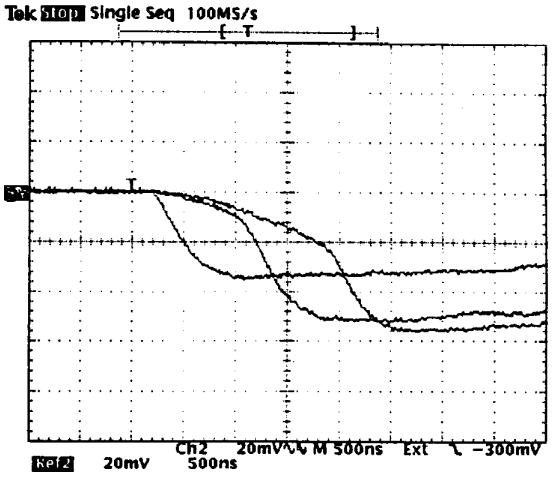

Figure 2: Charge signals resulting from full energy deposition in different points of the chamber.

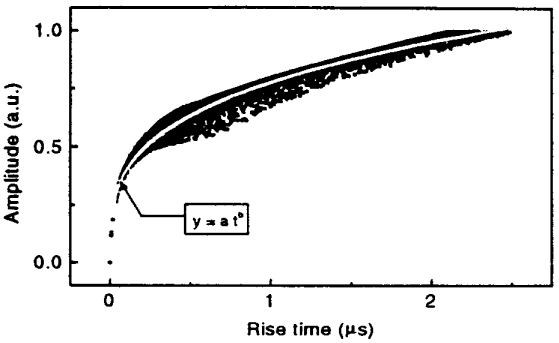

Figure 3: Simulated correlation plot between the charge signal amplitude and its rise time for monoenergetic events uniformly distributed in a cell [5].

PMTs (dynode signals) in coincidence with a scintillation detector (BaF_2 crystal of 5 cm diameter and 5 cm long coupled to a Philips XP2020Q photomultiplier). The crystal is placed under the cryostat and aligned with the ^{22}Na source, at a distance of about 25 cm from it.

III. Wire Signals: Amplitude Correction Algorithm and Induction Cross-Talk

A. Amplitude Correction Algorithm

In this ionisation chamber geometry, due to the low mobility of positive ions in the liquid, there is a strong dependence of both signal amplitude and shape on the point of

primary ionisation, which leads to the degradation of the energy resolution. This aspect was previously studied in detail by computing the shape of the charge signals on the wires in the liquid xenon chamber [5].

We now confirmed the calculation results experimentally, showing the dependence of the signal amplitude and shape on the position of gamma-ray interaction. The signal from each pair of wires was fed into an ICARUS charge sensitive preamplifier followed by ICARUS linear amplifiers [6] modified for a faster response time (rise time ≈300 ns). The preamplifiers have a r.m.s. noise of 400 electrons, a rise time of 300 ns and a decay time of 17 μs. The signals were observed with a digital oscilloscope (Tektronix TDS 380) triggered by the triple coincidences, i.e., coincidences between the two photomultipliers mounted in the liquid xenon chamber and the one coupled to the BaF_2 crystal. Fig.2. shows an example of wire signals resulting from full energy deposition for different ionisation positions inside the chamber. In order to ensure that they correspond to full energy deposition, i.e. 511 keV, one signal of maximum amplitude was selected for each rise time.

In principle, the effect of positive ions on the signals read from an ionisation chamber can be easily eliminated with an additional grid (Frisch grid) located in front of the collector [8]. However, in our case, this would involve considerable complication of the design and introduce an additional dead space between the anodes and the grid, which is highly undesirable. Therefore, alternative solutions are sought.

It was shown by Monte-Carlo simulation that there is a well-defined correlation between signal amplitude and rise time [5] (see Fig.3). From this correlation a formula was deduced, which allows the correction of the amplitude of the measured pulse from its dependence on the interaction position [5]:

$$A_{corrected} = \frac{A_{read}}{a\, t^{b}}, \qquad (1)$$

where A_{read} and t refer to the measured pulse amplitude and electron drift time, respectively, and a and b are adjustable parameters.

Simulation predicts a significant improvement in the energy resolution upon performing this correction [5].

B. Induction Cross-Talk

When the electrons are drifting towards the multiwire electrode, charge is induced not only on the collecting wire but also in the adjacent channel. Henceforth, this effect will be referred to as "induction cross-talk" and the pulse induced into the channel adjacent to the one where the charge is collected will be called "cross-talk pulse", for the sake of brevity. If these pulses are not suppressed, they will constitute an additional source of energy degradation. Furthermore, they will

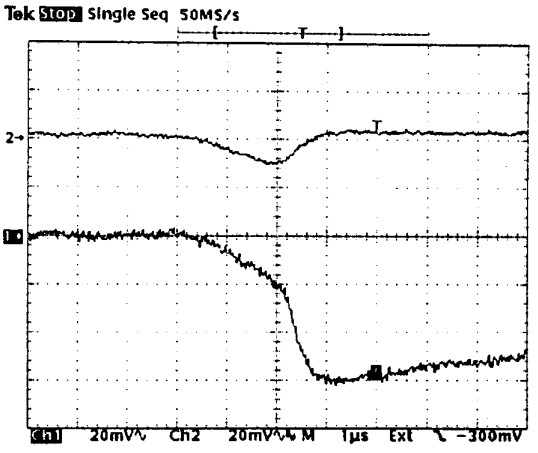

Figure 4: An example of the induction cross-talk: Channel 1 is the one in which drifting electrons are collected; channel 2 is the channel next to it.

prevent the unambiguous identification of events that, due to two or more interactions in the chamber, can also produce signals in adjacent channels. As discussed elsewhere [9], this type of events may eventually be used for image reconstruction. Therefore, care should be taken to correctly identify the channel into which the charge is collected.

Computation has shown that the shape of the charge signal in the collecting channel (a pair of wires) differs significantly from that of the pulse induced in the adjacent channel[5].

Fig.4 shows an example of the signals acquired in two adjacent channels, channel 1 being the one into which the drifting electrons are collected. While the electrons drift in the region far from the multiwire anode, they induce a similar signal in both channels; as they reach the region of converging electric field, they rapidly approach the collecting wire (producing the steep rise of the signal in channel 1) and move away from the other one (resulting in a decrease of the pulse amplitude in channel 2).

Thus, the identification of the charge collecting channel can be made on the basis of pulse shape discrimination, as we describe in section IV.D.

IV. Electronics and Data Acquisition System

A. Requirements

The readout electronics and the data acquisition system represented in Fig.5 were designed to fulfil the following requirements:

1. Provide triggering from coincidences between scintillation in the liquid xenon chamber and in the BaF_2 detector;

2. Measure the amplitude of the wires charge signals;

3. Suppress the cross-talk pulses.

4. Determine the rise time of the charge signals.

B. Trigger

In PET, the two back-to-back 511 keV γ-rays, resulting from the annihilation of a positron in the patient's body, have to be detected in fast coincidence, in order to make sure that they are correlated. In our case, the coincidence also enables rejection of the 1.27 MeV γ-rays out of the ^{22}Na source, as well as the background due to cosmic rays passing through the chamber.

Therefore, the signals from the three photomultipliers were fed in a coincidence unit (Philips Logic Unit 755). The signals from the PMTs installed in the chamber were taken from the last dynode, inverted and fed in constant fraction discriminators, CFD, (Philips TD 715). The threshold of the CFD was set at a voltage corresponding to 0.5 photoelectron [10]. The anode of the XP2020Q coupled to the BaF_2 scintillator was connected directly to a CFD, with the threshold corresponding to the γ-ray energy of 400 keV.

The output of the coincidence unit triggers the whole readout system, in particular it generates gates for the ADCs, starts the TDC's, strobes the register and initiates the acquisition cycle. At the same time, it vetoes the coincidence unit inputs until that cycle is finished, rejecting any scintillation light occurring in the meantime. All these aspects will be discussed in more detail in the subsections to follow.

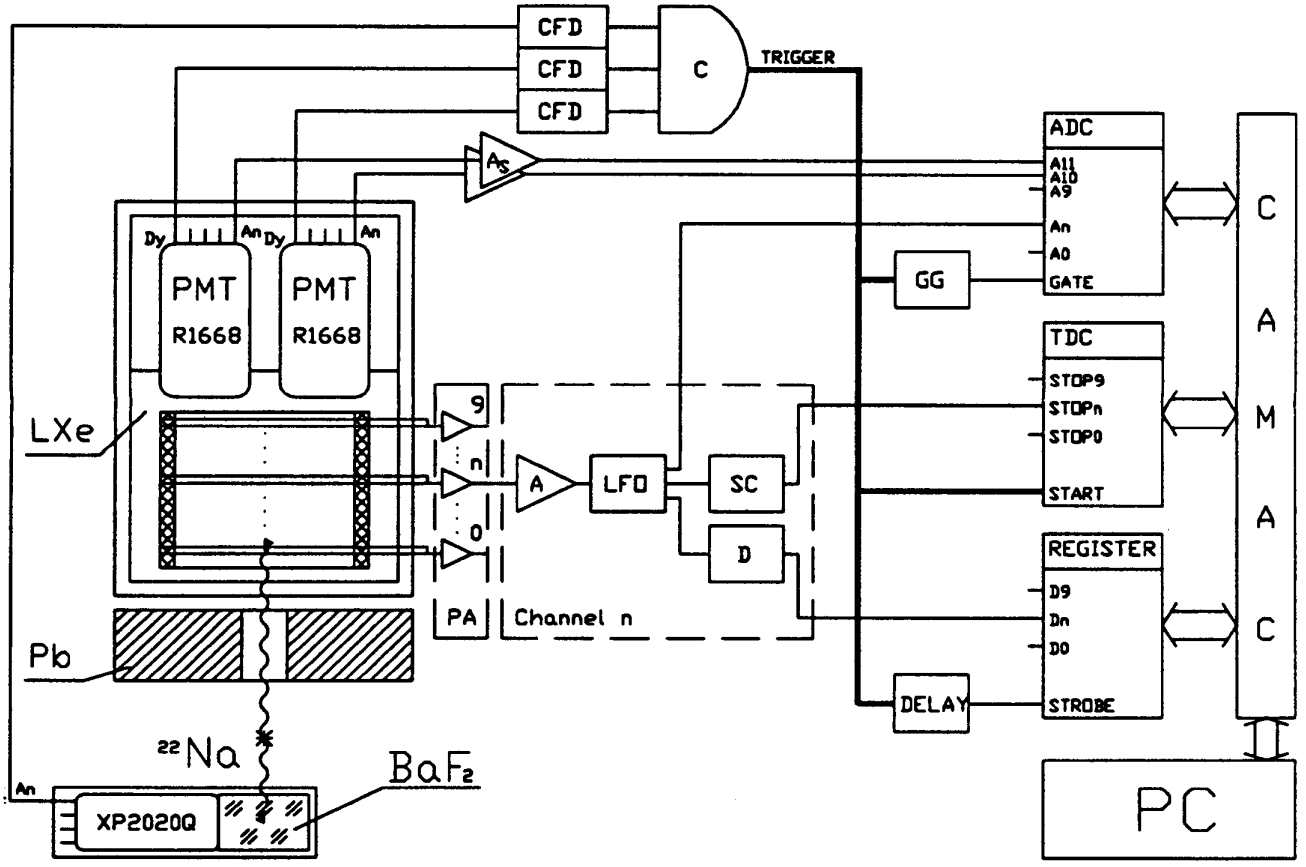

Figure 5: Block diagram of the readout and acquisition system for the liquid xenon chamber: PMT: photomultiplier (An and Dy are its anode and dynode outputs, respectively); PA: charge preamplifier; A: linear amplifier; A_s: shaping amplifier; CFD: constant fraction discriminator; C: coincidence unit; LFO: linear FAN-OUT; SC: Stop-circuit; D: discriminator; GG: gate generator; ADC: analogue to digital converter; TDC: time to digital converter; PC: IBM-type personal computer.

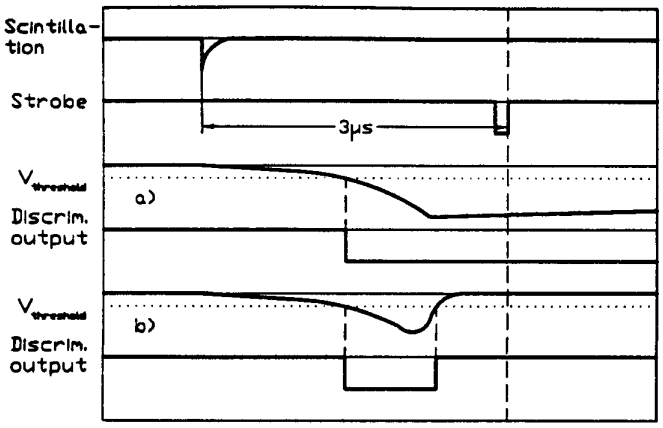

Figure 6: Pulse shape discrimination principle. a) Typical signal in the channel collecting the charge. b) Signal in the adjacent channel (cross-talk). In both cases the square waveform represents the output pulse of the discriminator which is fed with the charge signal.

C. Processing of charge signals

The signal from each pair of wires is processed by a separate electronics channel. In each channel, the signal is fed into a charge sensitive preamplifier followed by a linear amplifier, both of which have been described in detail in section III.A. As both the amplitude information and the rise time of the pulse should be retained, no shaping is performed in the amplifiers with the exception of a small integration of 0.1 μs for noise filtering. The signal from each amplifier is fed into a linear fan-out unit (LeCroy, 428F) from which three output signals are derived: one is fed in a peak sensing ADC (LeCroy ADC 2259B) for digitalisation of the pulse amplitude, another one goes into a timing circuit for determination of the pulse rise time (see section IV.E) and the third is fed to a discriminator for cross-talk rejection (see section IV.D).

D. Cross-talk rejection

A discriminator (Philips 711) was inserted in each channel for pulse shape discrimination. Its output is latched into a register (Caen C219) by a strobe signal occurring 3 μs after the trigger (see Fig.5). Hence, the latched value will be *1* in the case of a "real" signal, and *0* for a cross-talk signal, as shown in Fig.6. In our working conditions, the maximum collection time of electrons in the cell, which determines the longest signal rise time, is 2.5 μs (see Fig.9b) and the decay time of the signal is about 20 μs. After 3 μs the signal in the channel in which the charge is collected still has an amplitude above the threshold of the discriminator, while in case of a cross-talk signal the amplitude has already decreased well below the discriminator threshold. Therefore, a delay of 3 μs between the interaction instant and the cross-talk rejection decision moment is appropriate.

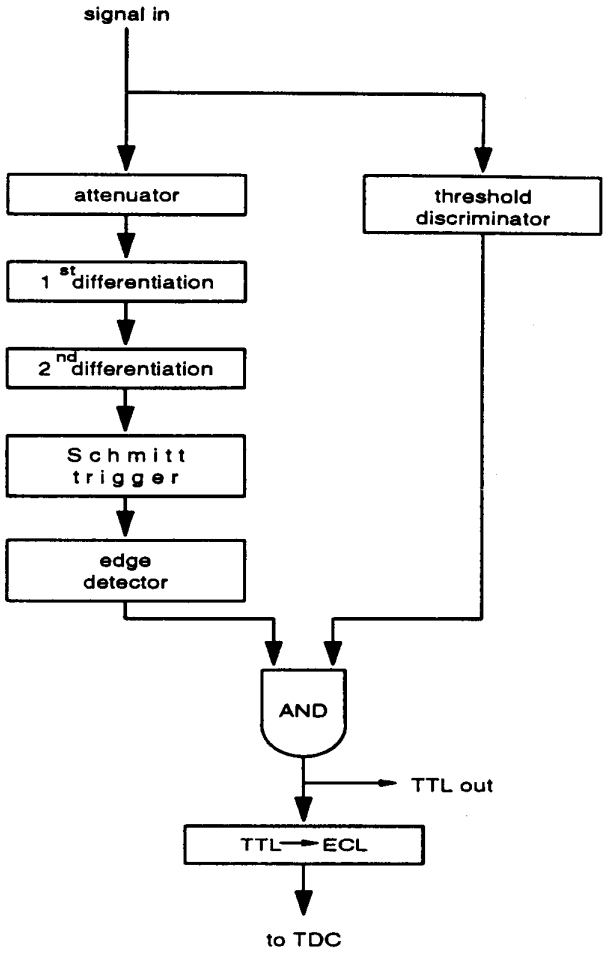

Figure 7: Functional lay-out of the stop-circuit

E. Timing

The drift time of the electrons is of utmost importance both for the determination of the *x*-coordinate of the interaction point of the γ-ray and for correction of the charge signal amplitude. Because the rise time of the charge pulses varies between ~100 ns and a few μs and the amplitude also varies over a rather wide range, standard timing techniques (CFD, ARC and SRT) are not appropriate. Due to the movement of the electrons in the high electric field region near the wire, all signals have in common a steep section at the end of the rise. In order to exploit this property a dedicated timing circuit has been built, whose functional lay-out is shown in Fig.7. The signals at various points of the circuit are shown in Fig.8.

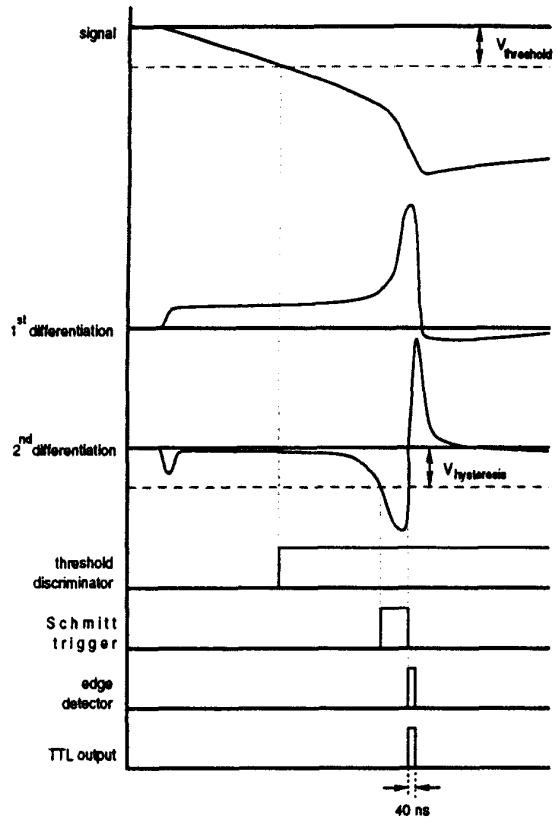

Figure 8: Timing diagram for the stop-circuit

The board has two active differentiators. For a better signal-to-noise ratio some integration has also been applied. The time constants for the differentiation and the integration have been optimised for the typical signal shape of our amplifiers (rise time ~300 ns). The active differentiators invert the polarity. The signal from the second differentiator is fed into a Schmitt trigger whose falling edge threshold was at the zero level. Its hysteresis was set large enough to avoid triggering on noise. Hence, if the leading edge of the signal exceeds the leading edge threshold of the Schmitt trigger, its output goes high, and it returns back to zero once the signal goes above the zero level. So, the negative going edge of the Schmitt trigger output indicates the actual zero crossing. An edge detector was accordingly placed after the Schmitt trigger, generating a short pulse of 40 ns width at the negative going edge.

The beginning of the signal causes a small peak in the second differentiation. To avoid a stop pulse to be produced at this peak, a threshold discriminator is used for the input signal. The outputs of this discriminator and of the edge detector are AND'ed together, so that a stop pulse is produced only when both signals are high. Finally, the TTL stop pulse is converted into an ECL pulse for the TDC.

The stop pulse has 40 ns width and is delayed by ~10 ns with respect to the real zero crossing. This delay is constant and can be easily accounted for in the correction. The amplifiers in each of the channels introduce an additional delay of ~360 ns. So, during the analysis a delay of 370 ns has to be subtracted from the measured drift time.

The time resolution has been tested with a pulser that produces pulses with amplitude and rise time of the same order of magnitude as those expected from the chamber. Time resolution appears to be somewhat dependent on amplitude, varying between 80 ns FWHM for signals of ~6,000 electrons and less than 20 ns FWHM for full charge signals (~30,000 electrons).

For measuring the rise time of the charge signals from the liquid xenon chamber, the output of the stop-circuit is fed to the STOP input of a TDC (CAMAC unit, LeCroy 22) whose START input is triggered from the output of the coincidence unit (see Fig. 5). The efficiency of the stop-circuit was measured to be about 92%, i.e. in 92% of the cases when charge is detected in a channel the board produces a stop-pulse. Signals that do not receive a stop-pulse generally have small amplitude.

F Data acquisition

The data acquisition system is controlled by a IBM-type personal computer, connected to the CAMAC controller by a GPIB link.

The data acquisition software reads the register status byte until a non-zero value is returned, which means that a STROBE pulse has arrived. Thus, the latched values at the register are read and analysed so that the ADC and TDC are read only for the channels corresponding to non-zero bits at the register, along with ADCs connected to the PMTs anodes (see Fig.5). The amplitude and timing information of those channels, the amplitude of the PMTs output signal, as well as the register bit pattern which allows identification of the channels where the collection of charge took place, are written in a file and constitute the data recorded for each event.

The analysis of the data acquired during a run is made off-line.

V. RESULTS

Measurements were performed with the described set-up. In Fig.9a a pulse height spectrum of the charge without correction is shown. Due to the positive ions, the resolution is very poor and no photoabsorption peak can be distinguished. Fig.9b represents a correlation plot between the measured charge signal amplitude and its rise time. The observed correlation is identical to the one obtained by computation (see Fig.3), although the distribution is broader. Nevertheless, two branches

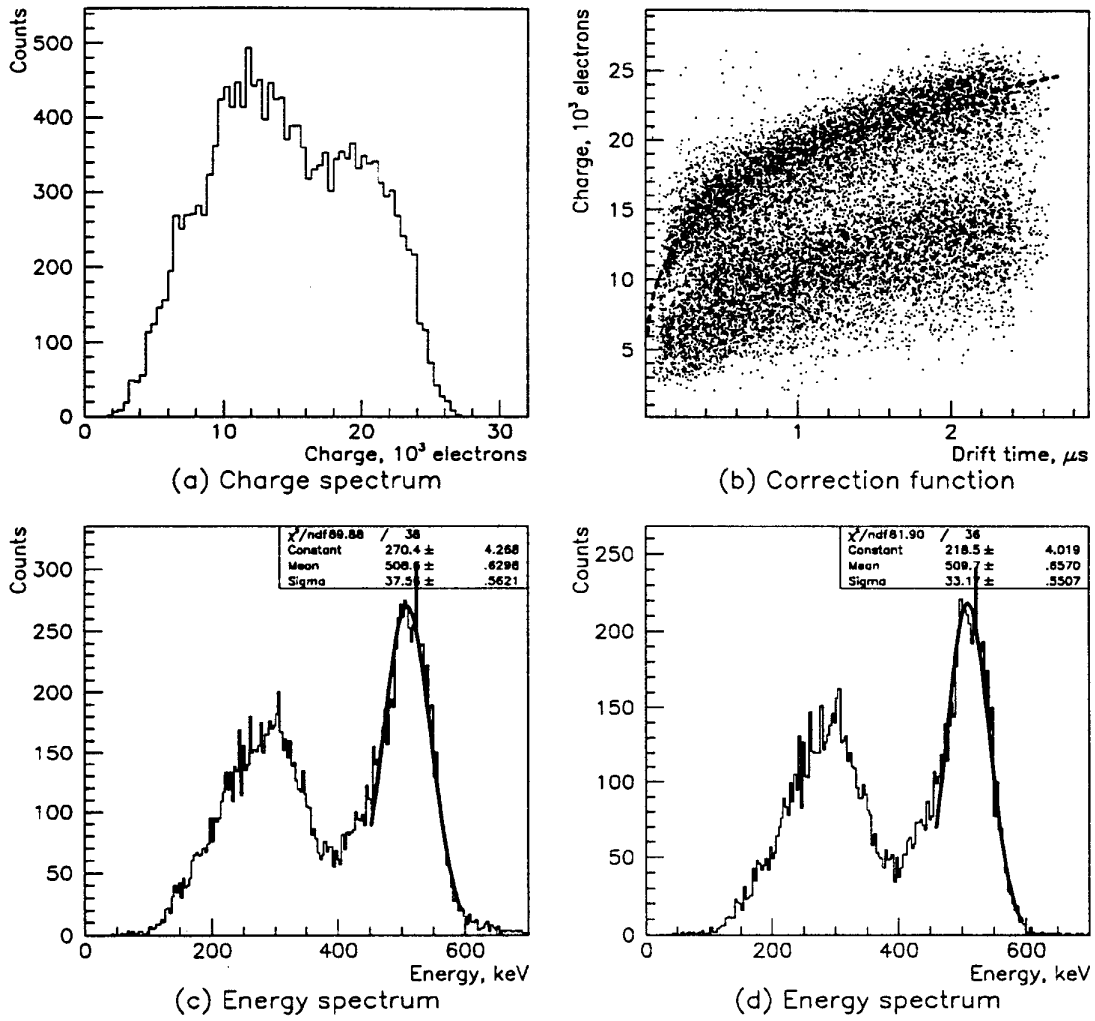

Figure 9: (a) Charge pulse height spectrum measured in a single wire; (b) measured charge as a function of drift time; (c) corrected spectrum taking all events; (d) corrected spectrum taking only the events with drift time >0.64 μs.

corresponding to photoabsorption and Compton scattering are clearly visible. Once the upper branch was fitted with function (1), the correction was applied to every pulse amplitude. The resulting spectra are shown in Fig.9c and Fig.9d. All events were taken into account in the spectrum displayed in Fig.9c, while in Fig.9d only those with drift time ≥0.64 μs were selected (25% events loss). The 511 keV photopeak is clearly distinguishable now. A gaussian fit gives an energy resolution of (17.2±0.2)% and (15.2±0.2)% fwhm, respectively.

As a simple alternative to the amplitude correction method, we have studied the possibility of using the current signal from the wires which is less affected by the positive ions. For that purpose, the wire charge signals were differentiated with a time constant varying in the range from 20 ns to 500 ns. Some integration with a smaller time constant has also been applied for noise filtering. The pulse height spectra acquired in this way were, in general, better than those obtained in charge mode without correction but worse than the ones corrected as described above.

VI. Conclusions

The system for reading out, processing and recording the charge signals from the liquid xenon chamber was designed

and successfully tested in real conditions. A special timing circuit for measuring the electron drift time was built. Information about drift time provides a way to correct the amplitude of the charge signal for the missing part due to the slowly moving positive ions. The correction leads to an energy resolution of 17% for 511 keV gamma rays (i.e. about 87 keV, fwhm), which is sufficient for efficient scatter rejection [11]. By rejecting events with drift time below 640 ns, the energy resolution is improved to 15%, at the expense of a 25% efficiency loss.

V. ACKNOWLEDGEMENTS

This work was carried out within the framework of the project PRAXIS XXI 2./2.1/SAU/1342/95. Some of the authors were supported by research grants: PRAXIS XXI/BPD/4135/94 PRAXIS XXI/BICJ/3847/97, PRAXIS XXI/BICJ/3848/97 and PRAXIS/4/4.1/BPD/4328. We also wish to thank the ICARUS group at CERN for useful discussions and for supplying the front-end electronics.

VI. REFERENCES

[1] V.Yu. Chepel, "A new liquid xenon scintillation detector for positron emission tomography", *Nucl.Tracks Rad. Meas.*, Vol.21, no1, pp. 47-51, 1993.

[2] V.Yu.Chepel, M.I.Lopes, H.M.Araújo, R.Ferreira Marques, M.A.Alves and A.J.P.L.Policarpo, "First tests of a liquid xenon multiwire drift chamber for PET", *Conference Record of the IEEE Nuclear Science Symposium and Medical Imaging Conference*, Norfolk, Virginia, USA, 1994, Ed. Robert C. Tendler, Vol.3, p.1155- 1159.

[3] V.Yu.Chepel, M.I.Lopes, H.M.Araújo, M.A.Alves, R.Ferreira Marques and A.J.P.L.Policarpo, "Liquid xenon multiwire chamber for positron tomography", *Nucl. Instr. and Meth. in Phys. Res.*, Vol.A367, pp.58- 61, 1995.

[4] V.Yu.Chepel, M.I.Lopes, A.Kuchenkov, R.Ferreira Marques and A.J.P.L.Policarpo. "Performance study of a liquid xenon detector for PET", *Nucl. Instr. and Meth. in Phys. Res.*, Vol.A397, pp.427-432, 1997.

[5] P.Crespo, V.Chepel, M.I.Lopes, L.Janeiro, R.Ferreira Marques and A.J.P.L.Policarpo. "Pulse shape analysis in the liquid xenon multiwire ionisation chamber for PET", *IEEE Trans. Nucl. Sci.*, Vol.45, no.3, pp.561-567, June 1998.

[6] TOTEM 2.2, developed by the ICARUS group at CERN; P. Benetti, A. Bettini, E. Calligarich et al., "A Three-ton liquid argon time projection chamber", *Nucl. Instr. and Meth. in Phys. Res.*, Vol.A332, pp.395-412, 1993.

[7] V.Y.Chepel, M.I.Lopes, R.Ferreira Marques and A.J.P.L. Policarpo, "Purification of liquid xenon and impurity monitoring for a PET detector", *Nucl. Instr. and Meth. in Phys. Res.*, Vol.A349, pp.500-505, 1994.

[8] G.Knoll, "Radiation detection and measurement", *New York: Wiley*, 1989 pp.154-155.

[9] M.I.Lopes, V.Yu.Chepel, J.C.Carvalho, R.Ferreira Marques and A.J.P.L. Policarpo, "Performance analysis based on a Monte-Carlo simulation of a liquid xenon PET detector", IEEE Trans. Nucl. Sci., Vol. 42, no. 6, pp.2298-2302, Aug.1995.

[10] V.Chepel, V.Solovov, J.van der Marel, M.I.Lopes, P.Crespo, L. Janeiro, Dinis Santos, R. Ferreira Marques and AJ.P.L. Policarpo, "The liquid xenon detector for PET: recent results", presented at *IEEE Nuclear Science Symposium and Medical Imaging Conference*, Toronto, Ontario, Canada, 1998.

[11] W.W. Moses, S.E. Derenzo, T.F. Budinger, "PET detector modules based on novel detector technologies", *Nucl. Instr. and Meth.*, A353 (1994) 189-194.